Supplementary Information

Explorations of Heteroatom Doping in Modulating the Two-electron Selectivity of M-N-C Catalysts for Oxygen Reduction Reaction

Zhou Huang,[a] Qisheng Yan[a] and Qing Tang*[a]

[a] School of Chemistry and Chemical Engineering, Chongqing Key Laboratory of Chemical Theory and Mechanism, Chongqing University, Chongqing 401331, China

*E-mail: qingtang@cqu.edu.cn

Computational Methods. All structural optimization calculations were performed using the Vienna Ab initio Simulation Package (VASP5.4.4)[1]. Electronic exchange-correlations were described using the Perdew-Burke-Ernzerhof (PBE) exchange-correlation functional[2] within the Generalized Gradient Approximation (GGA), while electron-ion interactions were treated using the Projector Augmented Wave (PAW) method[3]. The parameters for structural relaxation calculations were set as follows: the energy cutoff for the plane-wave basis set was set to 400 eV; the Brillouin zone was sampled using a 2 × 2 × 1 Monkhorst-Pack grid; and the convergence criteria for energy and force were 1×10^{-4} eV/atom and 0.01 eV/Å, respectively. Grimme's DFT-D3[4] correction was employed to account for van der Waals forces, ensuring the accuracy of interfacial interactions. When handling systems containing explicit water molecules at the interface, this study utilized a method termed the "Constant Potential Hybrid Solvation Dynamics Model" (CP-HS-DM) [5, 6] to calculate energy barriers under constant potential conditions. In this model, electrons are coupled to a fictitious potentiostat, allowing the Fermi level of the system to fluctuate around a constant value, while the number of electrons evolves according to a grand canonical distribution at the preset electrode potential. To maintain the electrical neutrality of the system, net charges are balanced by ionic charges in the implicit solvent. For constrained Ab Initio Molecular Dynamics (AIMD) simulations, the "slow growth" method was adopted, wherein the reaction coordinate transitions gradually from the

initial state to the final state. For each value of the reaction coordinate, the corresponding mean force acting on the reaction coordinate is extracted. By integrating the mean force with respect to the reaction coordinate, the free energy curve is obtained, from which the activation energy value is determined. The slow growth process calculations employed PBE-D3 with Becke-Jonson damping to describe van der Waals interactions, with a plane-wave basis set energy cutoff of 400 eV and a Brillouin zone sampling of a 1 × 1 × 1 Monkhorst-Pack grid.

The formation energy (E_f) is calculated as:

$$E_f = E_{M-sub} - \mu_M - E_{sub} \quad (1)$$

, where E_{M-sub} represents the energy of the clean substrate, E_{sub} is the total energy of structure without metal, μ_M is the energy of a single metal atom in the bulk phase.

The dissolution potential U_{diss} of metal atom is calculated by the following formula:

$$U_{diss} = U^{0}_{diss(metal,bulk)} - \Delta E_f/ne \quad (2)$$

, where $U^{0}_{diss(metal,bulk)}$ is the standard dissolution potential of the bulk metal, n is the number of electron transferred during dissolution. Only catalysts with E_f < 0eV and U_{diss} > 0V vs. SHE are considered to be both thermodynamically and electrochemically stable[7].

The ORR process was evaluated using the computational hydrogen electrode (CHE) model. The changes of Gibbs free energy (ΔG) for each ORR step can be calculated as

$$\Delta G = \Delta E + \Delta ZPE - T\Delta S + \Delta G_{pH} + \Delta G_U$$

where ΔE, ΔZPE, and ΔS are the changes of the total energy that can be directly obtained from DFT calculations, the difference of zero-point energy, and the change of entropy, respectively. ΔG_{pH} is the free energy change caused by the variation of the H^+ ion concentration, and the pH value was set to be 0. The temperature (T) was assumed to be 298.15 K in this work, and $\Delta G_U = -neU$, where n and U are the transferred electron numbers for each step and the electrode potential, respectively.

The zero-point energy and entropy of the free H_2 and H_2O molecules were obtained according to the NIST database. Then, the calculated results are ΔZPE_{H_2O} = 0.57 eV, $T\Delta S_{H_2O}$= 0.58 eV, ΔZPE_{H_2} = 0.27 eV, and $T\Delta S_{H_2}$= 0.45 eV. Given the difficulty in the calculation of the free energy of H_2O(l), we adopted a correction of 0.09 eV under 0.035 bars as the reference state because, at this pressure, the liquid and gas phases of H_2O can reach equilibrium at 298.15 K. Thus, the final entropic term of H_2O(l) was 0.67 eV (0.58 + 0.09 = 0.67 eV).

The detailed pathway for 2*e* mechanism in ORR was adopted in our work as the following two steps:

$$O_2 + H^+ + e^- \rightarrow *OOH$$

$$*OOH + H^+ + e^- \rightarrow * + H_2O_2$$

the reaction free energy can be calculated by:

$$\Delta G_1 = G_{*OOH} - 1.5G_{H_2} - G_{O_2} + eU$$

Owing to the high-spin ground state of the O_2 molecule, it is poorly described in DFT computations. To avoid calculating the energy of O_2, we first calculated reaction free energy of equations $*+ 2H_2O \rightarrow *OOH + 3/2H_2$

Then, the reaction free energy can be defined as:

$$\Delta G_{*OOH} = 1.5G_{H_2} + G_{*OOH} - 2G_{H_2O} - G_*$$

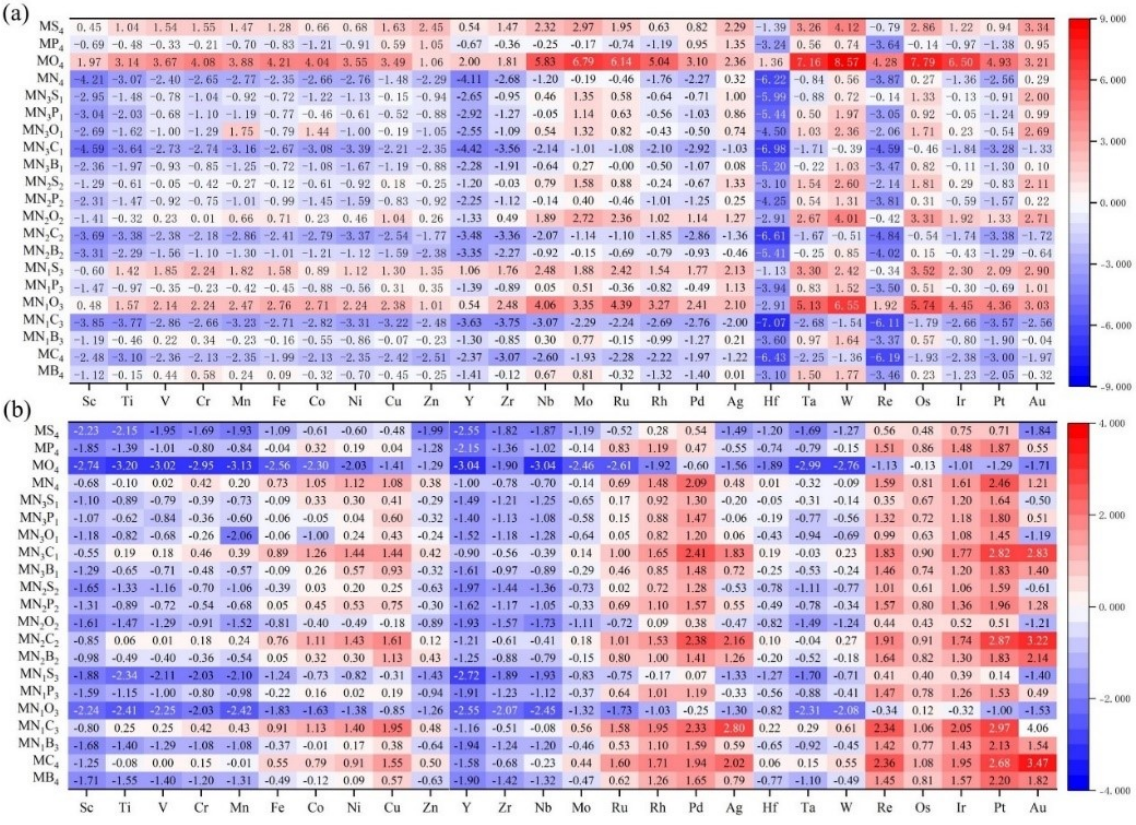

Fig.S1 Metal atomic formation energy (E_f) (a) and dissolution potential (U_{diss}) (b) of pyridine-nitrogen coordinated single-atom catalysts.

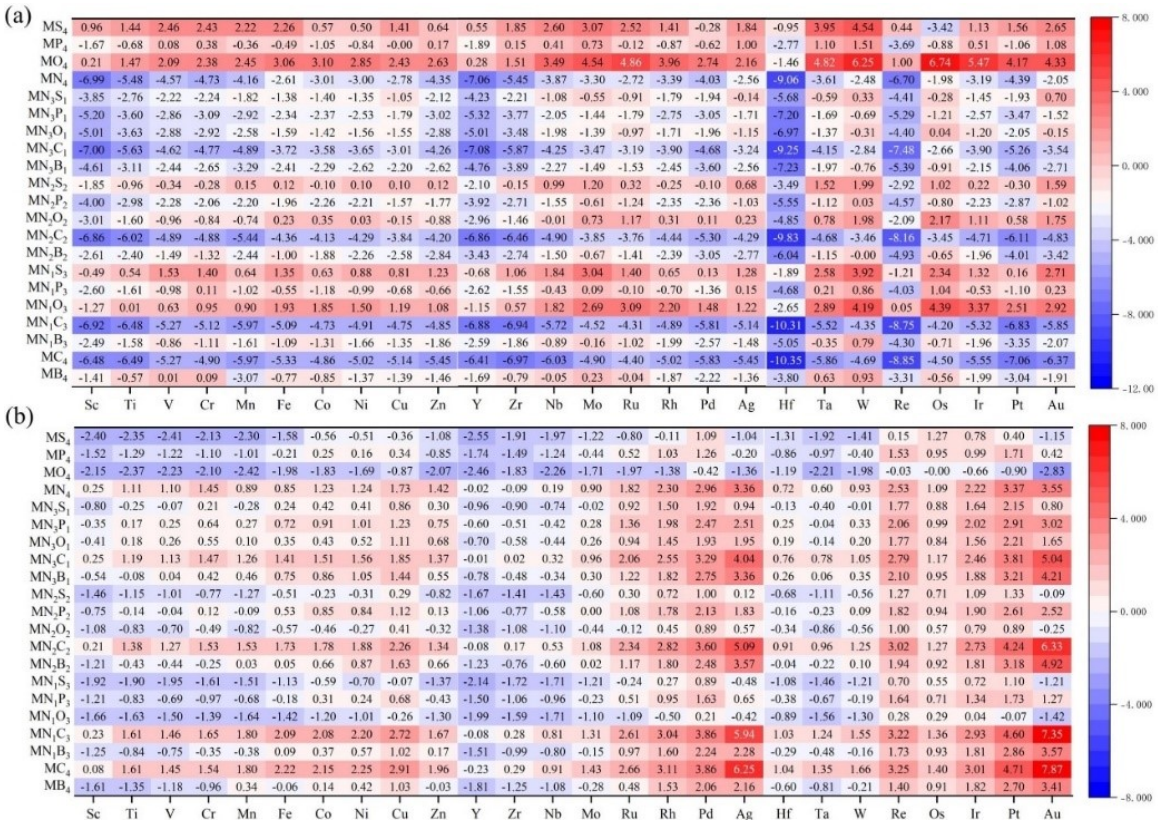

Fig.S2 Metal atomic formation energy (E_f) (a) and dissolution potential (U_{diss}) (b) of pyrrole-nitrogen coordinated single-atom catalysts.

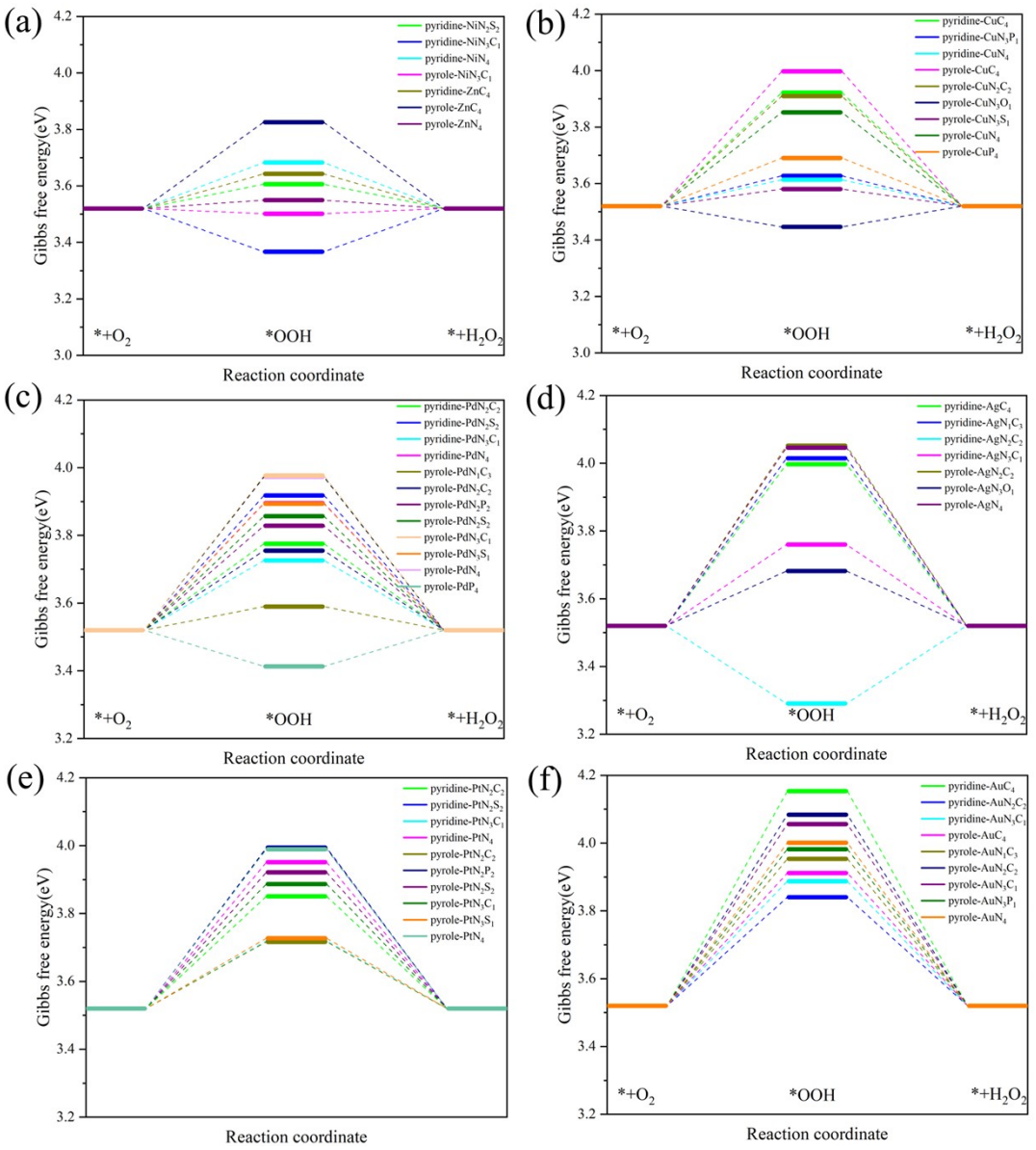

Fig.S3 Free energy diagrams of the two-electron pathway of 54 single-atom catalysts screened at the equilibrium potential of 0.7 V.

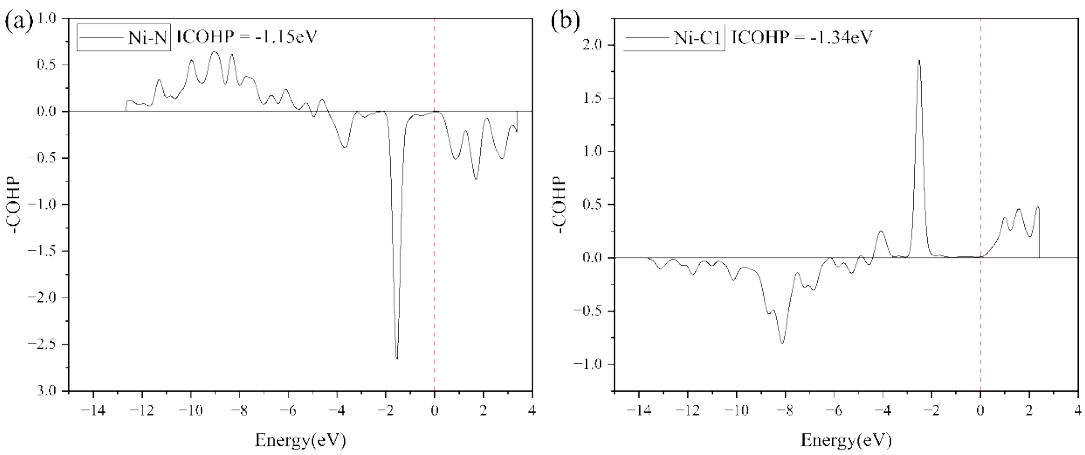

Fig.S4 The COHP plots and ICOHP values of Ni-N (a) in pyridine-type NiN_4 and Ni-C (b) in pyrrole-type NiN_3C_1.

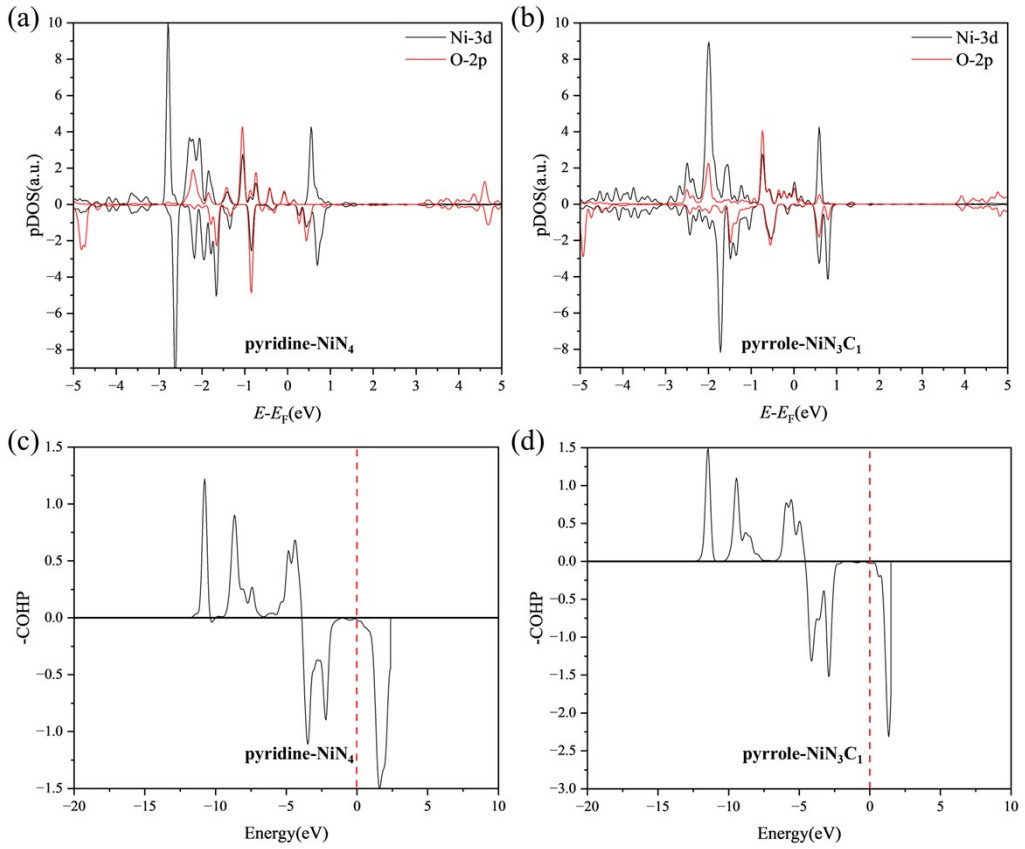

Fig.S5 Partial density of states (PDOS) diagrams of metal Ni and O in (a) pyridine-type NiN_4*OOH and (b) pyrrole-type NiN_3C_1*OOH. COHP plot of metal Ni and O in (c) pyridine-type NiN_4*OOH and (d) pyrrole-type NiN_3C_1*OOH.

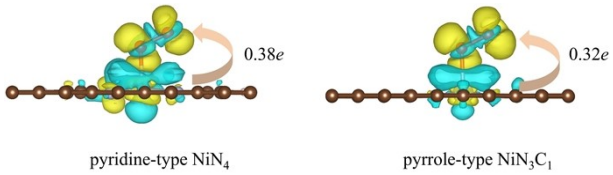

Fig.S6 The charge density difference plot and the charge transfer of pyridine-type NiN_4*OOH and pyrrole-type NiN_3C_1*OOH.

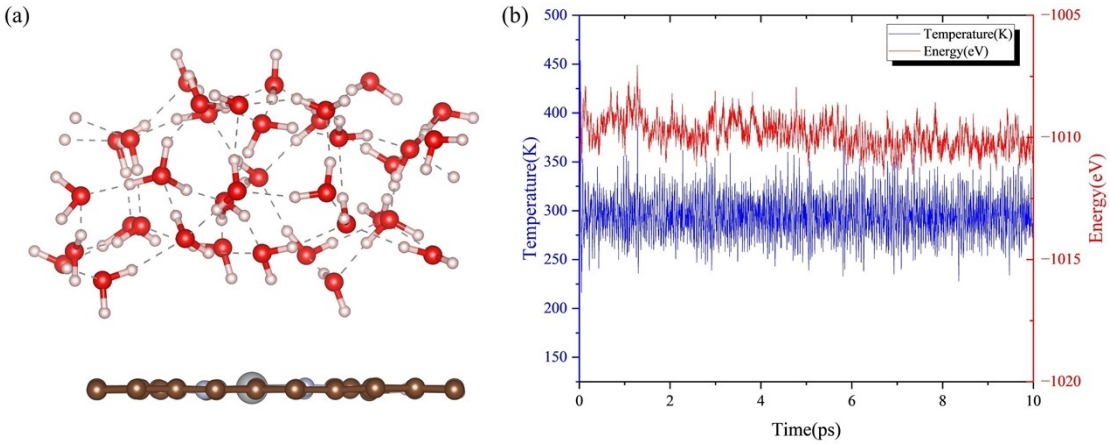

Fig.S7 (a) The snapshot structures of pyrrolic-type NiN_3C_1 after 10 ps MD simulations; (b) MD energy and temperature profiles for pyrrolic-type NiN_3C_1 during 10 ps AIMD simulations.

References

1 G. Kresse and D. Joubert, *Phys. Rev. B*, 1999, **59**, 1758.
2 J. P. Perdew, K. Burke and M. Ernzerhof, *Phys. Rev. Lett.*, 1996, **77**, 3865.
3 P. E. Blöchl, *Phys. Rev. B*, 1994, **50**, 17953.
4 S. Grimme, S. Ehrlich and L. Goerigk, *J. Comput. Chem.*, 2011, **32**, 1456-1465.
5 X. Zhao and Y. Liu, *J. Am. Chem. Soc.*, 2021, **143**, 9423-9428.
6 S. Yu, Z. Levell, Z. Jiang, X. Zhao and Y. Liu, *J. Am. Chem. Soc.*, 2023, **145**, 25352-25356.
7 J. Greeley and J. K. Nørskov, *Electrochim. Acta*, 2007, **52**, 5829-5836.